DOCUMENT CONTROL SHEET

	ORIGINATOR'S REF.		SECURITY CLASS.
	NLR TP 96283 U		Unclassified

ORIGINATOR
National Aerospace Laboratory NLR, Amsterdam, The Netherlands

TITLE
Adaptive generation of structured grids
Part II: Weighted Least Squares formulation

PRESENTED AT
the VKI lecture series: 27th Computational Fluid Dynamics, March 25-29, 1996, Von Karman Institute, Rhode-Saint-Genèse, Belgium

AUTHORS	DATE	pp	ref
R. Hagmeijer, J.C. Kok	960325	32	23

DESCRIPTORS

Adaption	Euler-Lagrance equation	Three dimensional flow
Aerodynamic coefficients	Grid generation (mathematics)	Transonic
Algorithms	Orthogonality	Weighting functions
Boundary value problems	Reynolds number	Wings
Boundary layers	Structured grids (mathematics)	

ABSTRACT
Based on a general Weighted Least Squares formulation a family of grid adaptation equations is defined. Some methods from the literature are reviewed within this WLS frame work. To satisfy a number four formulated requirements a compound WLS approach is presented. This part of the lecture is based on references [1], [2], [3] and [4]. The adaptation algorithm is applied to an airfoil and a wing in transonic flow.

NLR TECHNICAL REPORT

TP 96283 U

ADAPTIVE GENERATION OF STRUCTURED GRIDS

Part 2

Weighted Least Squares Formulation

by

R. Hagmeijer and J.C. Kok

This paper has been presented at the VKI lecture series: 27th Computational Fluid Dynamics, March 25-29, 1996, Von Karman Institute, Rhode-Saint-Genèse, Belgium.

Division : Fluid Dynamics
Prepared : RH/ JCK/
Approved : BO/

Completed : 960325
Order number : 526.501
Typ. : LMT

Contents

This page is intentionally left blank

Adaptive Generation of Structured Grids, Part2

Rob Hagmeijer and Johan Kok
National Aerospace Laboratory NLR, The Netherlands
tel 31-20-5113459; fax 31-20-5113210; e-mail hagm@nlr.nl
VKI Lecture series: 27th Computational Fluid Dynamics

25-29 March 1996

Abstract

Based on a general Weighted Least Squares formulation a family of grid adaptation equations is defined. Some methods from the literature are reviewed within this WLS frame work. To satisfy a number four formulated requirements a compound WLS approach is presented. This part of the lecture is based on references [1], [2], [3], and [4]. The adaptation algorithm is applied to an airfoil and a wing in transonic flow.

1 Weighted Least Squares (WLS) Formulation

1.1 Introduction

The present section aims at extending the principles presented in Part 1 of this lecture towards a formulation that is suitable for three-dimensional problems. The objective in Part 1 was to map the interval $[0, L] \subset \mathcal{R}$ to the unit interval $[0, 1] \subset \mathcal{R}$, whereas in this section the objective is to map the three-dimensional physical domain $\Omega \subset \mathcal{R}^3$ to the unit cube $[0, 1]^3 \subset \mathcal{R}^3$. Once such a map is constructed, say $\xi(x)$, the inverse of that map, $x(\xi)$, can be used to map a uniform rectangular grid in the unit cube to a curvilinear grid in the physical domain Ω.

As a preparation it is first described how the physical domain $\Omega \subset \mathcal{R}^3$ is mapped to the unit interval. This map is based on a weighted least squares (WLS) formulation. Then it is derived how the map of Ω to the unit cube is constructed by combination of three separate maps from Ω to the unit interval. In section 1.3 a number of examples from the literature is discussed cast within the presented WLS formulation.

1.2 Map of $\Omega \subset \mathcal{R}^3$ to the unit interval

The objective is to construct a map $\phi(x)$ from $\Omega \subset \mathbf{R}^3$ to the unit interval:

$$\phi(x): \quad \Omega \subset \mathbf{R}^3 \mapsto [0, 1], \tag{1}$$

such that iso-surfaces can be used as one family of coordinate surfaces belonging to a map from $\Omega \subset \mathbf{R}^3$ to the unit cube.

Let the functional $K[\phi]$ be defined on a bounded domain $\Omega \subset \mathcal{R}^3$ with Cartesian coordinates $\mathbf{x} = (x, y, z)^T$:

$$K[\phi] = \frac{1}{2} \int_\Omega \frac{1}{w_j(\mathbf{x})} (\mathbf{h}_j(\mathbf{x}) \cdot \nabla\phi)^2 \, d\Omega, \tag{2}$$

where the Einstein summation convention is applied and $\mathbf{h}_j(\mathbf{x}) \in R^3 \, (j = 1, 2, 3)$ and $\nabla = (\frac{\partial}{\partial x}, \frac{\partial}{\partial y}, \frac{\partial}{\partial z})$. In (2) $w_j \, (j = 1, 2, 3)$ are bounded strictly positive functions of the physical coordinates:

$$w_j(\mathbf{x}): \quad \Omega \in \mathcal{R}^3 \mapsto [\delta, \infty); \quad \delta > 0, \quad j = 1, 2, 3, \tag{3}$$

and it is assumed that the $\mathbf{h}_j(\mathbf{x})$ are nonzero and independent.

Functional K in (2) can be considered as an extension of the equidistribution principle for 1D problems, see functional (11), Part 1, which incorporates the derivative of the object funtion, $\xi(x)$, with respect to the physical coordinate x. As an extension, functional K given by (2) incorporates three different components of the gradient of the object function ϕ determined by the vector functions $\mathbf{h}_j(\mathbf{x})$, $j = 1, 2, 3$. In addition, the single weight function $w(x)$ incorporated in functional (11), Part 1, is replaced by three separate weight functions $w_j(\mathbf{x})$, $j = 1, 2, 3$, in functional K given by (2) to enable anisotropic weighting of the components of the gradient of ϕ.

K can be rewritten in matrix vector notation:

$$K[\phi] = \frac{1}{2} \int_\Omega (M \nabla\phi) \cdot \nabla\phi \, d\Omega, \tag{4}$$

where M is a symmetric 3x3 matrix:

$$M = H \, W^{-1} \, H^T, \quad H = (\mathbf{h}_1 \, \mathbf{h}_2 \, \mathbf{h}_3), \quad W = diag(w_1, w_2, w_3). \tag{5}$$

From (2) and the assumption that the $\mathbf{h}_j(\mathbf{x})$ are nonzero and independent it follows that the integrand of K is positive for any $\nabla\phi \neq 0$. Because M is real and symmetric it follows that M is positive definite (see e.g. ref. [5]).

Let on a part $\partial\Omega^D \subset \partial\Omega$ the function ϕ be specified:

$$\phi = \phi_0, \quad \mathbf{x} \in \partial\Omega^D, \tag{6}$$

then we will consider the following variational problem:

Variational Problem 1.1 *Find a function* $\phi(\mathrm{x}): \quad \Omega \subset \mathrm{R}^3 \mapsto \mathrm{R}$ *with* $\phi(\mathrm{x}) = \phi_0(\mathrm{x})$ *for* $\mathrm{x} \in \partial\Omega^D \subset \partial\Omega$ *such that the functional* $K[\phi]$ *given by (4) is minimized.*

Although we could refer to [6] and immediately state the equations that have to be satisfied by the function ϕ to extremize functional $K[\phi]$ given by (4), we prefer to present a derivation of these equations to direct attention to the fact that not only the Euler-Lagrange (EL) equation has to be satisfied but also the associated **natural boundary condition.**

Let $\tilde{\phi}$ be an arbitrary function within the class of admissible perturbation functions of the solution ϕ. Then:

$$K[\phi + \varepsilon\tilde{\phi}] = K[\phi] + \varepsilon \int_\Omega (M\nabla\phi) \cdot \nabla\tilde{\phi}\, d\Omega + \varepsilon^2 K[\tilde{\phi}], \quad \varepsilon \in \mathcal{R}. \tag{7}$$

The term that is linear in ε is the first variation of K that can be evaluated using the Divergence Theorem:

$$\int_\Omega (M\nabla\phi) \cdot \nabla\tilde{\phi}\, d\Omega = -\int_\Omega \tilde{\phi}\nabla \cdot (M\nabla\phi)\, d\Omega + \int_{\partial\Omega} \tilde{\phi}\mathbf{n} \cdot (M\nabla\phi)\, d\Gamma. \tag{8}$$

If K is minimized by the function ϕ then the condition

$$\frac{\partial K}{\partial \varepsilon}(\varepsilon = 0) = 0, \tag{9}$$

must be satisfied, hence the first variation (8) must be zero. Since both integrals at the right hand side of (8) involve the arbitrary function $\tilde{\phi}$, both integrals must be zero. The first integral at the right hand side of (8) is zero for all admissible functions $\tilde{\phi}$ if and only if its integrand is zero, resulting in the Euler-Lagrange (EL) equation (ref. [6]):

$$\nabla \cdot (M\nabla\phi) = 0, \quad \mathrm{x} \in \Omega. \tag{10}$$

Equation (10) is a second-order linear partial differential equation (PDE) which is elliptic since M is positive definite. If the smallest eigenvalue of M has a lower positive bound in Ω, the EL equation is even uniformily elliptic and the extremum principle of Hopf is valid (refs. [5],[7]).

The second integral at the right hand side of (8) is also zero for all admissible functions $\tilde{\phi}$ if and only if its integrand is zero. On the part $\partial\Omega^D$ of the boundary where ϕ is specified $\tilde{\phi}$ must be identically zero such that the compound function $\phi + \varepsilon\tilde{\phi}$ satisfies the same specification. On the remaining part $\{\partial\Omega \setminus \partial\Omega^D\}$ $\tilde{\phi}$ is not neccesarily zero resulting in the so-called *natural boundary condition* (ref. [6]):

$$\mathbf{n} \cdot (M\nabla\phi) = 0, \quad \mathrm{x} \in \{\partial\Omega \setminus \partial\Omega^D\}, \tag{11}$$

where $\mathbf{n} \in \mathcal{R}^3$ denotes the outward unit normal on $\partial\Omega$. The combined conditions (10) and (11) are sufficient to extremize the functional K. Since M is positive definite the term in (7) that is quadratic in ε is non-negative. Hence:

$$K[\phi + \varepsilon\tilde{\phi}] \geq K[\phi] \tag{12}$$

with equality if and only if $\varepsilon = 0$. This proves that the stationary point of K is unique and consists of a minimum.

To relate the present analysis to formulations found in the literature the question arises whether it is possible to formulate functional K as a WLS functional in case M is a arbitrary positive definite matrix. Since M is real and symmetric there exists an orthogonal matrix R such that $\Lambda = R^{-1} M R$ is a diagonal matrix and the column vectors $\mathbf{r}_j$ $(j = 1, 2, 3)$ of R form an orthogonal set of eigenvectors of M (ref. [5]). Because R is orthogonal $R^{-1} \equiv R^T$ and the eigenvectors are orthonormal:

$$\mathbf{r}_i \cdot \mathbf{r}_j = \delta^{ij}, \tag{13}$$

where δ^{ij} is the Kronecker delta. With these relations M can be decomposed:

$$M = R\Lambda R^T, \quad R = (\mathbf{r}_1\,\mathbf{r}_2\,\mathbf{r}_3), \quad \Lambda = diag(\lambda_1, \lambda_2, \lambda_3), \tag{14}$$

where λ_j $(j = 1, 2, 3)$ are the eigenvalues of M which are real and positive because M is positive definite. Hence the following WLS formulation is always possible:

$$K[\phi] = \frac{1}{2}\int_\Omega (M\nabla\phi)\cdot\nabla\phi\, d\Omega = \frac{1}{2}\int_\Omega \lambda_j\,(\mathbf{r}_j\cdot\nabla\phi)^2\, d\Omega, \tag{15}$$

A key element of the present problem formulation is the required compatibility of the natural boundary condition (11) with the frequently applied generalized Neumann boundary condition:

$$\tau\cdot\nabla\phi = 0, \quad x \in \{\partial\Omega \setminus \partial\Omega^D\}, \tag{16}$$

where τ is a vector with a non-zero component in the direction of the unit outward normal:

$$\tau\cdot\mathbf{n} \neq 0, \tag{17}$$

If (16) is applied it must be equivalent with (11) to make the functional K stationary. Because M is symmetric

$$\mathbf{n}\cdot(M\nabla\phi) = (M\mathbf{n})\cdot\nabla\phi \tag{18}$$

leading to the following *compatibility condition*:

$$M\mathbf{n} = \lambda\tau, \quad \lambda \neq 0, \quad x \in \{\partial\Omega \setminus \partial\Omega^D\}. \tag{19}$$

In the special case that τ is identical to $\mathbf{n}$, then $\mathbf{n}$ must be an eigenvector of M on $\{\partial\Omega\setminus\partial\Omega^D\}$. Condition (19) imposes important restrictions on the construction of candidates for M.

1.3 Applications from the literature

1.3.1 Laplace maps

Brackbill and Saltzmann (ref. [8]) used a compound functional within a variational problem formulation for adaptive grid generation consisting of three functionals: one for smoothness, one for orthogonality and one for adaptation. In this section we will discuss only the smoothness functional:

$$I_S[\xi,\eta,\zeta] = \frac{1}{2}\int_\Omega \{\|\nabla\xi\|^2 + \|\nabla\eta\|^2 + \|\nabla\zeta\|^2\}\, d\Omega, \tag{20}$$

This functional can be written in WLS format (4) as:

$$I_S[\xi,\eta,\zeta] = K[\xi] + K[\eta] + K[\zeta], \tag{21}$$

with

$$K[\phi] = \frac{1}{2}\int_\Omega (M\nabla\phi)\cdot\nabla\phi\, d\Omega, \quad M = \begin{pmatrix} 1 & 0 & 0 \\ 0 & 1 & 0 \\ 0 & 0 & 1 \end{pmatrix}. \tag{22}$$

The EL equations (10) result in the Laplace equation for each of the computational coordinates ξ, η and ζ:

$$\nabla\cdot(\nabla\xi) = 0, \quad \nabla\cdot(\nabla\eta) = 0, \quad \nabla\cdot(\nabla\zeta) = 0, \quad \mathbf{x} \in \Omega. \tag{23}$$

1.3.2 Isotropic diffusion (ID) maps

Winslow (ref. [9]) introduced a single weight function into the smoothness functional of Brackbill and Saltzmann to account for smoothness as well as for adaptation. The functional is:

$$I[\xi,\eta,\zeta] = \frac{1}{2}\int_\Omega \frac{1}{w(\mathbf{x})}\{\|\nabla\xi\|^2 + \|\nabla\eta\|^2 + \|\nabla\zeta\|^2\}\,d\Omega. \tag{24}$$

This functional can be written in WLS format (4) as:

$$I[\xi,\eta,\zeta] = K[\xi;w] + K[\eta;w] + K[\zeta;w], \tag{25}$$

with

$$K[\phi;w] = \frac{1}{2}\int_\Omega (M\nabla\phi)\cdot\nabla\phi\,d\Omega, \quad M = \frac{1}{w}\begin{pmatrix} 1 & 0 & 0 \\ 0 & 1 & 0 \\ 0 & 0 & 1 \end{pmatrix}. \tag{26}$$

The EL equations (10) consist of identical isotropic diffusion equations for each of the computational coordinates ξ, η and ζ:

$$\nabla\cdot(\frac{1}{w}\nabla\xi) = 0, \quad \nabla\cdot(\frac{1}{w}\nabla\eta) = 0, \quad \nabla\cdot(\frac{1}{w}\nabla\zeta) = 0, \quad \mathbf{x}\in\Omega. \tag{27}$$

1.3.3 Weakly related isotropic diffusion (WRID) maps

Eiseman [10] introduced an interesting extension to the approach of Winslow [9] by using different weight functions $w_j(\mathbf{x})$, $j = 1,2,3$, one for each coordinate direction, to enable anisotropic grid adaptation. The functional is:

$$I[\xi,\eta,\zeta] = \frac{1}{2}\int_\Omega \{\frac{1}{w_1}\|\nabla\xi\|^2 + \frac{1}{w_2}\|\nabla\eta\|^2 + \frac{1}{w_3}\|\nabla\zeta\|^2\}\,d\Omega, \tag{28}$$

This functional can be written in WLS format (4) as:

$$I[\xi,\eta,\zeta] = K[\xi;w_1] + K[\eta;w_2] + K[\zeta;w_3], \tag{29}$$

with $K[\phi;w]$ defined by (26). The EL equations (10) consist of weakly related isotropic diffusion equations, one for each of the computational coordinates ξ, η and ζ:

$$\nabla\cdot(\frac{1}{w_1}\nabla\xi) = 0, \quad \nabla\cdot(\frac{1}{w_2}\nabla\eta) = 0, \quad \nabla\cdot(\frac{1}{w_3}\nabla\zeta) = 0, \quad \mathbf{x}\in\Omega. \tag{30}$$

these equations are weakly related by the assumption that the weight functions $w_j(\mathbf{x})$, $j = 1,2,3$, are different though all derived from the same scalar or vector function (e.g. an initial guess of the flow solution).

1.3.4 Harmonic maps

Harmonic maps with user-specified metric tensors for grid adaptation have been introduced by Dvinsky (ref. [11]) and reviewed by Brackbill (ref. [12]). In the present section harmonic maps are discussed within the frame work of the WLS formulation.

Let the functional E_0 be defined as:

$$E_0[\phi] = \frac{1}{2}\int_\Omega d^{ij}\frac{\partial\phi}{\partial x^i}\frac{\partial\phi}{\partial x^j}\sqrt{d}\,d\Omega, \tag{31}$$

where d^{ij} is the user-specified symmetric contravariant metric tensor in the coordinates $\mathbf{x}$ and $d = det\{d_{ij}\} > 0$. The covariant metric tensor of the Eucledian coordinates in the unit cube is the identity

matrix and hence does not show up in the functional E_0. E_0 can be rewritten in the matrix vector format (4):

$$E_0[\phi] = \frac{1}{2}\int_\Omega (M\nabla\phi)\cdot\nabla\phi\, d\Omega, \quad M^{ij} = \sqrt{d}\, d^{ij}. \tag{32}$$

The generation of an adaptive grid in Ω can be considered as a map from a three-dimensional Riemannian manifold in $\mathcal{R}^4$ described by the local coordinates x to the unit cube. The additional dimension with respect to $\Omega \subset \mathcal{R}^3$ can be obtained by defining a function Q on Ω to which the grid must be adapted (ref. [13]):

$$\Phi : \Omega \mapsto \mathcal{R}^4, \quad \Phi(x,y,z) = (x,y,z,Q(x,y,z))^T. \tag{33}$$

The Jacobian of the map (33) is:

$$J_\Phi = (\Phi_x, \Phi_y, \Phi_z)^T, \tag{34}$$

and hence the covariant tensor d_{ij} is:

$$d_{ij} = (J_\Phi J_\Phi{}^T)^{ij} = \delta^{ij} + \frac{\partial Q}{\partial x^i}\frac{\partial Q}{\partial x^j}, \quad d = det\{d_{ij}\} = 1 + \|\nabla Q\|^2. \tag{35}$$

The characteristic equation for the eigenvalues of d_{ij} is:

$$(\bar{\lambda} - d)(\bar{\lambda} - 1)^2 = 0, \tag{36}$$

with solutions $\bar{\lambda}_1 = d$ and $\bar{\lambda}_2 = 1$ respectively. The eigenspace belonging to $\bar{\lambda}_1$ is one-dimensional and is spanned by ∇Q, the gradient of Q. The eigenspace belonging to $\bar{\lambda}_2$ is two-dimensional and consists of all vectors in three-dimensional space that are normal to ∇Q. Hence, the metric tensor $\sqrt{d}\, d^{ij}$ has the same eigenspaces with eigenvalues $\lambda_1 = d^{-\frac{1}{2}}$ and $\lambda_2 = d^{\frac{1}{2}}$ respectively. Written in terms of the eigenvalues and eigenspaces of the matrix M the WLS formulation of E_0 is:

$$E_0[\phi] = \frac{1}{2}\int_\Omega \frac{1}{\sqrt{d}}(\mathrm{r}_1.\nabla\phi)^2 + \sqrt{d}\,\{(\mathrm{r}_2.\nabla\phi)^2 + (\mathrm{r}_3.\nabla\phi)^2\}\, d\Omega, \tag{37}$$

where the eigenvectors r_i $(i = 1,2,3)$ form an orthonormal set and $\mathrm{r}_1 = \frac{\nabla Q}{\|\nabla Q\|}$.

The harmonic map is established by minimizing the 'total energy' functional:

$$E[\xi,\eta,\zeta] = E_0[\xi] + E_0[\eta] + E_0[\zeta], \tag{38}$$

The EL equations associated with the minimization of $E[\xi,\eta,\zeta]$ are:

$$L_{LB}(\xi) = 0, \quad L_{LB}(\eta) = 0, \quad L_{LB}(\zeta) = 0, \tag{39}$$

where L_{LB} is the Laplace-Beltrami operator.

1.3.5 Discussion

We state the following requirements to be fulfilled by any adaptation method based on WLS formulation:

1. *The three PDE's that are derived from the chosen functional must be identical.* The regularity theorem that is presented in section 2.5 is based on the assumption that the PDE's for each of the computational coordinates are identical. Since the regularity of a map from $\Omega \subset \mathrm{R}^3$ to the unit cube depends on the relationship between the three computational coordinates it seems inevitable to require that the three PDE's be identical.

2. *the PDE's must resemble anisotropic adaptation.* To enable an effective and efficient grid adaptation algorithm it should be possible to stretch cells differently in different directions.

Table 1: Comparison of WLS maps used in the literature

Maps	Anisotropic?	M clear?	Compatiblity?	Identical PDE's?
Laplace	no	yes	yes	yes
ID	no	yes	yes	yes
WRID	yes	no	yes	no
Harmonic	yes	yes	no	yes

3. *The matrix M must be a function of x only.* If the matrix M is not a function of x alone but also a function of ξ then the PDE's derived in the previous sections are not the EL-equations associated with the formulated variational problems.

4. *The compatibility condition (19) must be satisfied.* To impose ordinary Neumann conditions and simultaneously minimise the chosen functional, the compatibility condition must be satisfied.

The various maps presented in sections 1.3.1 to 1.3.4 can be discussed in view of the above formulated four requirements.

Laplace maps. The PDE's that are derived from the smoothness functional in section 1.3.1 are all identical Laplace equations and are hence isotropic. The matrix M is the identity matrix and the compatibility condition (19) is satisfied.

Isotropic diffusion maps. The PDE's that are derived from the functional formulated by Winslow, see section 1.3.2, are identical isotropic diffusion equations. The matrix M is the identity matrix multiplied by a scalar function w, hence the compatibility condition (19) is satisfied. Requirement 3) can be satisfied by definition of w as a function of x only.

Weakly related Isotropic diffusion maps. The PDE's that are derived from the functional formulated by Eiseman, see section 1.3.3, are not identical isotropic diffusion equations. The three matrices are identity matrices multiplied by the scalar functions w_i, $i = 1, 2, 3$, hence the compatibility condition (19) is satisfied. Looking at expression (28) for the functional to be minimized, the weight functions w_i, $i = 1, 2, 3$, are used to weigh the gradients $\|\nabla\xi^i\|$, $i = 1, 2, 3$. hence it is natural to choose the weight functions as a norm of the gradient component of some function, e.g. the flow solution, in the direction of ξ^i. This implies , however, that the weight functions w_i, $i = 1, 2, 3$, are not functions of x only but are also functions of ξ, the solution of the variational problem. As a consequence equations (30) are not the EL-equations associated with functional (28).

Harmonic maps. The PDE's that are derived from the functional formulated by Dvinsky, see section 1.3.4, are anisotropic and identical. The matrix is well-defined and expression (37) for the functional to be minimized enables a clear interpretation.

The component of $\nabla\phi$ in the direction ∇Q at one hand and the components of $\nabla\phi$ normal to ∇Q at the other hand are weighted with inversely proportional weights. These are consequences of the objective to generate a smooth grid in the Riemannian manifold formed by the four-dimensional vector field $(x, y, z, Q)^T$.

A complete extension to multiple functions Q_i, $i = 1, 2, .., N$ can be derived in a similar manner (ref. [13]). However, there is an important drawback: the compatibility condition (19) is not satisfied by the metric tensor $\sqrt{d}\, d^{ij}$ for arbitrarily chosen functions Q. Hence if Neumann conditions are imposed along the domain boundary the functional E is not minimized and the claim to generate the smoothest possible map on the monitor surface can not be substantiated.

The satisfaction of requirements 1) to 4) formulated above, is summarized in table 1. The conclusion is that none of the discussed WLS functionals presented in the literature satisfy all of the requirements 1) to 4). This is the motivation for the work presented in the next section; the construction of a WLS functional that satisfies all four requirements.formulated above.

2 Compound WLS maps

2.1 Objective

The objective of the present section is to construct a compound WLS functional that satisfies all of the four requirements formulated in section 1.3.5. The idea is to map the physical domain to the unit cube by means of an auxiliary parametric map resulting in a parametrisation of the physical space Ω. The resulting parametric map can be chosen such that the compatibility condition (19) is satisfied.

Subsequently the auxiliary parametric domain, say Ω_p, is mapped by a WLS map to another unit cube which is the computational domain Ω_c. Hence, the map from the physical domain Ω to the computational domain Ω_c is constructed as a compound map consisting of two underlying maps, see Fig. 1.

The compound WLS map has the following prospects:

1. If some map from the physical domain Ω to the unit cube is already available it can directly be used as the auxiliary map. This is the usual situation for grid adaptation; the existing grid that has to be adapted implicitly defines the auxiliary map to the unit cube.

2. Since the WLS map to be constructed maps the unit cube onto itself, the matrix in the WLS functional can conveniently be chosen as a diagonal matrix.

3. If Neumann boundary conditions are imposed on the boundary of the parametric domain, and if the WLS map between the parametric domain and the computational domain is described by a WLS functional involving a diagonal matrix, the compatibility condition is satisfied. This is explained in the next section.

One of the benefits of the variational formulation is the ability to interpret the resulting PDE's. In section 2.3 it is described how the compound WLS functional can be rewritten to resemble the Equidsribution Principle for multi-dimensional problems. In addition it is shown in section 2.4 that the EL equations associated with the compound WLS functional can be written as averaged 1D Equidistribution Principles. Finally, section 2.5 describes an invertibility theorem for 2D problems.

2.2 General formulation

We start by formulating the WLS functional that upon minimization defines the WLS map between the parametric domain Ω_p and the computational domain Ω_c. Let the functional $K[\phi]$ be defined as:

$$K[\phi] = \frac{1}{2}\int_{\Omega_p} (W^{-1}\nabla_p\phi)\cdot\nabla_p\phi \, d\Omega_p, \tag{40}$$

where W is a 3x3 diagonal matrix with strictly positive diagonal elements w_i, $i = 1,2,3$. With this functional the following variational problem is defined:

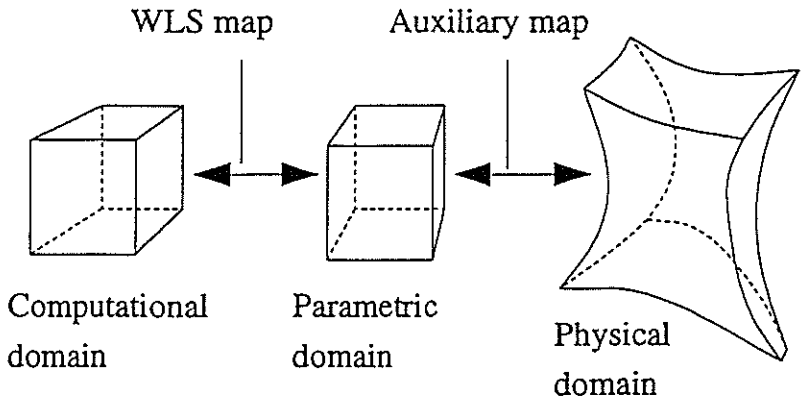

Figure 1: Schematic visualisation of compound WLS map.

Variational Problem 2.1 *Find a function* $\phi(\mathrm{p}): \quad \Omega_p \subset \mathrm{R}^3 \mapsto \mathrm{R}$ *with* $\phi(\mathrm{p}) = \phi_0(\mathrm{p})$ *for* $\mathrm{p} \in \partial\Omega_p^D \subset \partial\Omega_p$ *such that the functional* $K[\phi]$ *given by (40) is minimized.*

From section 1.2 we know that problem 2.1 is solved if the EL-equation

$$\nabla_p \cdot (W^{-1}\nabla_p\phi) = 0, \quad \mathrm{p} \in \Omega_p, \tag{41}$$

is solved while on that part of the boundary where no Dirichlet conditions are imposed the associated natural boundary conditions are imposed:

$$\mathrm{n}_p \cdot (W^{-1}\nabla_p\phi) = 0, \quad \mathrm{p} \in \{\partial\Omega_p \setminus \partial\Omega_p^D\}, \tag{42}$$

where $\mathrm{n}_p \in \Omega_p$ denotes the outward unit normal on $\partial\Omega_p$. Since W is a diagonal matrix the EL-equation does not contain mixed partial derivatives. Since that Ω_p is a unit cube this enables a clear interpretation of the functional $K[\phi]$, see sections 2.3 and 2.4.

It is further noted that because W is a diagonal matrix the natural boundary condition (42) is compatible with the ordinary Neumann condition since the compatibility condition (19) is satisfied on the complete boundary $\partial\Omega_p$:

$$W^{-1}\mathrm{n}_p = \lambda \mathrm{n}_p, \tag{43}$$

where $\lambda = w_1^{-1}$ on boundaries $p = 0$ and $p = 1$, $\lambda = w_2^{-1}$ on boundaries $q = 0$ and $q = 1$, and $\lambda = w_3^{-1}$ on boundaries $r = 0$ and $r = 1$. Hence, the natural boundary condition may be replaced by the ordinary Neumann condition:

$$\mathrm{n}_p \cdot \nabla_p\phi = 0, \quad \mathrm{p} \in \{\partial\Omega_p \setminus \partial\Omega_p^D\}. \tag{44}$$

For the physical domain this means that the compatibility condition (19) is satisfied if one of the column vectors of $J = (\mathrm{x}_p, \mathrm{x}_q, \mathrm{x}_r)^T$ that is not coinciding with $\partial\Omega$ is used to specify the generalized Neumann condition (16):

$$\mathrm{x}_s \cdot \nabla\phi = 0, \quad \mathrm{x} \in \{\partial\Omega \setminus \partial\Omega^D\}, s \in \{p, q, r\}. \tag{45}$$

In other words, the natural boundary condition associated with the variational problem in the physical domain is fully determined by the auxiliary map $\mathrm{x}(\mathrm{p})$. So the construction of the map $\mathrm{x}(\mathrm{p})$ can be used to control the generalized Neumann conditions that are compatible with these natural boundary conditions.

Before formulating the complete boundary value problem that governs grid adaptation it is useful to note that functional K given by (40) can be expressed in the physical domain Ω as:

$$K[\phi] = \frac{1}{2}\int_\Omega \{\frac{(\mathrm{x}_p \cdot \nabla\phi)^2}{w_1} + \frac{(\mathrm{x}_q \cdot \nabla\phi)^2}{w_2} + \frac{(\mathrm{x}_r \cdot \nabla\phi)^2}{w_3}\}\frac{d\Omega}{|J|}, \tag{46}$$

This form explicitily reveals the WLS character since the components of the gradient of ϕ in the directions of iso-parametric curves of the auxiliary parametric map are weighted with separate weight functions. From this observation it followsd that the obvious choice is to take the weight functions in terms of derivatives of the monitor function(s) along the iso-parametric curves.

It is also noted that the functional K given by (40) can be expressed in the parametric domain Ω_p in the compact form:

$$K[\phi] = \frac{1}{2}\int_{\Omega_p} \{\frac{\phi_p^2}{w_1} + \frac{\phi_q^2}{w_2} + \frac{\phi_r^2}{w_3}\}\, d\Omega_p, \tag{47}$$

The complete boundary value problem formulation for adaptive grid generation can conveniently be formulated in the parametric domain Ω_p, based on minimization of the compound functional:

$$I_{CWLS}[\xi, \eta, \zeta] = K[\xi] + K[\eta] + K[\zeta], \tag{48}$$

with Dirichlet boundary conditions

$$\begin{array}{l} \xi(0,q,r)=0,\ \xi(1,q,r)=1, \\ \eta(p,0,r)=0,\ \eta(p,1,r)=1, \\ \zeta(p,q,0)=0,\ \zeta(p,q,1)=1. \end{array} \tag{49}$$

To solve this variational problem the associated EL equations

$$L(\xi^{(k)}) = \frac{\partial}{\partial p}(\frac{\xi_p^{(k)}}{w_1}) + \frac{\partial}{\partial q}(\frac{\xi_q^{(k)}}{w_2}) + \frac{\partial}{\partial r}(\frac{\xi_r^{(k)}}{w_3}) = 0,\ k = 1,2,3, \tag{50}$$

must be solved subjected to a set of additional natural boundary conditions:

$$\begin{array}{l} \xi_q(p,0,r)=0,\ \xi_q(p,1,r)=0,\ \xi_r(p,q,0)=0,\ \xi_r(p,q,1)=0, \\ \eta_p(0,q,r)=0,\ \eta_p(1,q,r)=0,\ \eta_r(p,q,0)=0,\ \eta_r(p,q,1)=0, \\ \zeta_p(0,q,r)=0,\ \zeta_p(1,q,r)=0,\ \zeta_q(p,0,r)=0,\ \zeta_q(p,1,r)=0, \end{array} \tag{51}$$

Hence the objective to satisfy all of the conditions discussed in section 1.3.5 is met:

- The PDE's are anisotropic,
- The formulation of the matrix M is clear,
- The compatibility condition is satisfied, and
- The PDE's are identical.

2.3 Multiple 1D equidistribution interpretation in Ω_p

To demonstrate the connection between the variational problem formulated in section 2.2 and the *Equidistribution Principle* presented in Part 1 of this lecture we will show that there exists an equivalent variational problem that involves functionals that explicitly express the *Equidistribution Principle*.

Consider the following functional:

$$\hat{K}[\phi, \mathbf{c}] = \frac{1}{2}\int_{\Omega_p} (W(W^{-1}\nabla_p\phi - \mathbf{c}))\cdot(W^{-1}\nabla_p\phi - \mathbf{c})\, d\Omega_p, \tag{52}$$

with $\mathbf{c} \in \mathcal{R}^3$ constant. If we express it in scalar notation:

$$\hat{K}[\phi, c] = \frac{1}{2}\int_{\Omega_p} \sum_{i=0}^{3} w_i(\frac{1}{w_i}\frac{\partial\phi}{\partial p^{(i)}} - c^{(i)})^2\, d\Omega_p, \tag{53}$$

the connection to the *Equidistribution Principle* is revealed.

Without proof we state that the EL equation is:

$$\nabla_p \cdot (W^{-1}\nabla_p\phi - \mathbf{c}) = 0, \quad \mathbf{p} \in \Omega_p \tag{54}$$

and the expression for the natural boundary condition is:

$$\mathbf{n} \cdot (W^{-1}\nabla_p\phi - \mathbf{c}) = 0, \quad \mathbf{p} \in \partial\Omega_p \setminus \partial\Omega_p^D, \tag{55}$$

see also section 1.2. Because $\mathbf{c}$ is a constant the EL-equation (54) associated with functional $\hat{K}$ is equivalent with the EL-equation (41) associated with functional K. To obtain equivalence of the natural boundary conditions (55) and (52) it is required that the following condition be satisfied:

$$\mathbf{n} \cdot \mathbf{c} = 0, \quad \mathbf{p} \in \partial\Omega_p \setminus \partial\Omega_p^D. \tag{56}$$

For the problem formulation for the first computational coordinate $\xi = \xi^{(1)}$ condition (56) is satisfied if we take $\mathbf{c}$ of the form $\mathbf{c} = (c_1, 0, 0)^T$. For the problem formulations for η and ζ similar expressions can

be derived such that we are in a position to formulate the complete equivalent problem with respect to the functional I_{CWLS} (48) and boundary conditions (49). Retaining the boundary conditions (49) we replace I_{CWLS} by $\hat{I}_{CWLS}$ defined as:

$$\hat{I}_{CWLS}[\xi,\eta,\zeta,c_1,c_2,c_3] = \hat{K}[\xi,c_1] + \hat{K}[\eta,c_2] + \hat{K}[\zeta,c_3]. \tag{57}$$

As shown above this functional has the same EL-equations (50) and natural boundary conditions (51) as the original functional I_{CWLS} in (48). To interpret the new functional $\hat{I}_{CWLS}$ we evaluate it to:

$$\hat{I}_{CWLS}[\xi,\eta,\zeta,c_1,c_2,c_3] = \frac{1}{2}\int_{\Omega_p}\{w_1(\frac{\xi_p}{w_1}-c_1)^2 + w_2(\frac{\xi_q}{w_2})^2 + w_3(\frac{\xi_r}{w_3})^2$$

$$+ w_1(\frac{\eta_p}{w_1})^2 + w_2(\frac{\eta_q}{w_2}-c_2)^2 + w_3(\frac{\eta_r}{w_3})^2 + w_1(\frac{\zeta_p}{w_1})^2 + w_2(\frac{\zeta_q}{w_2})^2 + w_3(\frac{\zeta_r}{w_3}-c_3)^2\}\,d\Omega_p. \tag{58}$$

This expression reveals the multiple equidistribution character of the problem formulation because minimization of functional $\hat{I}_{CWLS}$ means that all terms in the integrand will be small in some optimal sence, with a tendency towards:

$$\frac{\xi_p}{w_1} \to c_1, \quad \xi_q \to 0, \quad \xi_r \to 0,$$

$$\eta_p \to 0, \quad \frac{\eta_q}{w_2} \to c_2, \quad \eta_r \to 0,$$

$$\zeta_p \to 0, \quad \zeta_q \to 0, \quad \frac{\zeta_r}{w_3} \to c_3. \tag{59}$$

Hence the variational problem formulated in section 2.2 tends to satisfy three separate 1D equidistrbution principles where each of the three computational coordinates ξ, η and ζ are preferably adapted separately.

2.4 Averaged 1D equidistribution interpretation in Ω_p

Another way to show the connection between the 1D Equidistribution Principle and the variational problem formulated in section 2.2 is to integrate the EL-equations (50) over q and r ($k=1$), over p and r ($k=2$) and over p and q ($k=3$) by using the natural boundary conditions (51). The result consists of three expressions:

$$\frac{\partial}{\partial p}\int_0^1\int_0^1 \frac{\xi_p}{w_1}\,dq\,dr = 0, \tag{60}$$

$$\frac{\partial}{\partial q}\int_0^1\int_0^1 \frac{\eta_q}{w_2}\,dp\,dr = 0, \tag{61}$$

$$\frac{\partial}{\partial r}\int_0^1\int_0^1 \frac{\zeta_r}{w_3}\,dp\,dq = 0. \tag{62}$$

These expressions directly reveal the 1D Equidistribution Principle connection.

2.5 Invertibility theorem for 2D problems

A critical aspect of grid generation and grid adaptation is the ability of the applied algorithm to provide grids that only incorporate cells with positive volumes. In other words the map from the computational domain to the physical domain must be one-to-one and have a Jacobian that is strictly positive everywhere execpt for a finite number of points where it may be zero. Assuming that these conditions are met by the map between the parametric domain and the physical domain it remains to be shown that the adaptive map between the computational domain and the parametric domain also satisfies these conditions. For the 2D case where the computational and parametric domains both consist of the unit square it can be proven that for a large class of elliptic partial differential equations with appropriate boundary conditions the

map is invertible. The relevant theorem has recently been developed by Clement, Hagmeijer and Sweers [14] within the frame work of grid adaptation research and is explicitly listed here.

Let the open unit square $(0,1)\times(0,1)$ in $\mathcal{R}^2$ be denoted by S and the sides by Γ_1 to Γ_4 in the following way:

$$\begin{cases} \Gamma_1 = \{0\} \times (0,1), \\ \Gamma_2 = (0,1) \times \{1\}, \\ \Gamma_3 = \{1\} \times (0,1), \\ \Gamma_4 = (0,1) \times \{0\} \end{cases}$$

Consider the problem:

$$(a) \begin{bmatrix} Lu = 0 & in & S, \\ u = 0 & on & \Gamma_1, \\ u = 1 & on & \Gamma_3, \\ \frac{\partial u}{\partial n} = 0 & on & \Gamma_2 \cup \Gamma_4, \end{bmatrix} \quad and \quad (b) \begin{bmatrix} Lv = 0 & in & S, \\ v = 1 & on & \Gamma_2, \\ v = 0 & on & \Gamma_4, \\ \frac{\partial v}{\partial n} = 0 & on & \Gamma_1 \cup \Gamma_3, \end{bmatrix} \tag{63}$$

where we are looking for a solution $(u,v) \in W^{2,p}(S) \times W^{2,p}(S)$ with $p \in (2,\infty)$. For a domain in $\mathcal{R}^2$ with a Lipschitz boundary one has $W^{2,p}(S) \subset C^1(\bar{S})$ $p > 2$, see Theorem 7.26 of [15].

The operator L in (63) is given by:

$$L = a_1(x,y)\frac{\partial^2}{\partial x^2} + a_2(x,y)\frac{\partial^2}{\partial y^2} + b_1(x,y)\frac{\partial}{\partial x} + b_2(x,y)\frac{\partial}{\partial y}, \tag{64}$$

where the coefficients satisfy for some $c > 0$ and $\gamma \in (0,1)$

$$a_i \in C^{0,1}(\bar{S}), a_i \geq c > 0 \quad in \quad \bar{S}, \quad i = 1,2, \tag{65}$$

and

$$b_i \in C^{\gamma}(\bar{S}), \quad i = 1,2. \tag{66}$$

Theorem 1 *Problem 63 possesses exactly one solution $(u,v) \in C^2(\bar{S})$. Moreover (u,v) is a bijection from $\bar{S}$ (resp. S) onto itself and*

$$det \begin{pmatrix} u_x & u_y \\ v_x & v_y \end{pmatrix} > 0 \quad on \quad \bar{S}.$$

The proof of theorem 1 is several pages long [14] and is not repeated here. The main fundament of the proof is the use of the Carleman-Hartman-Wintner (CHW) Theorem (see [16]) which describes the structure of a solution to second order PDE's in the neighbourhood of critical points. Mainly because there is no straightforward higher dimensional extension of the CHW-Theorem it is not expected that theorem 1 can be extended to hold for the three dimensional cube.

3 Applications

3.1 Modified equations in the parametric domain: 2D

A disadvantage of grid adaptation in the parametric domain is the possible generation of excessive skew cells in the physical domain when the initial grid contains cells with aspect ratios that are much smaller or larger than one. To illustrate this, let ϕ be the angle between two lines of the adapted grid in the physical domain Ω with constant ξ and η, respectively, and let the initial grid in Ω be orthogonal:

$$\mathbf{x}_p \cdot \mathbf{x}_q = 0. \tag{67}$$

The angle ϕ can be expressed in terms of derivatives with respect to the computational coordinates ξ and η:

$$\phi = \arccos\left(\frac{\mathbf{x}_\xi \cdot \mathbf{x}_\eta}{\|\mathbf{x}_\xi\| \, \|\mathbf{x}_\eta\|}\right), \tag{68}$$

which upon substitution of the functions $p(\xi,\eta)$ and $q(\xi,\eta)$ can be written as

$$\phi = \arccos\left(\frac{p_\xi p_\eta + \alpha^2 q_\xi q_\eta}{\sqrt{p_\xi^2+\alpha^2 q_\xi^2}\sqrt{p_\eta^2+\alpha^2 q_\eta^2}}\right), \tag{69}$$

where α is proportional to the local aspect ratio of the initial grid:

$$\alpha = \frac{\|\mathbf{x}_q\|}{\|\mathbf{x}_p\|}. \tag{70}$$

From (69) it can be deduced that when the adapted grid in the parametric domain Ω_p is nearly ortogonal, i.e.,

$$\mathbf{p}_\xi \cdot \mathbf{p}_\eta = p_\xi p_\eta + q_\xi q_\eta \ll \sqrt{p_\xi^2 + q_\xi^2}\sqrt{p_\eta^2 + q_\eta^2} = \|\mathbf{p}_\xi\|\,\|\mathbf{p}_\eta\|, \tag{71}$$

the adapted grid in Ω is also nearly orthogonal when $\alpha \approx 1$. However, when $\alpha \ll 1$ or $\alpha \gg 1$ Eq. (69) shows that $\phi \approx 0$ when $p_\xi\, p_\eta \neq 0$ or $q_\xi\, q_\eta \neq 0$ respectively; i.e., the adapted grid in Ω is collapsed. Cells of large or small aspect ratios within the field of CFD occur commonly in boundary layers. Most Navier-Stokes solvers need orthogonal grids in boundary layers; i.e., grid lines are required to originate from solid surfaces in the normal direction. Moreover, gradients in the normal direction are much larger than gradients in the tangential direction. Hence it is desirable that the grid in the boundary layer is primarily adapted in the normal direction and that the adaptation in the tangential direction is constrained by the orthogonality requirement. To obtain this property of the adaptation algorithm, the adaptation equations (50) are modified:

$$\lambda_1 \frac{\partial}{\partial p}\frac{\xi_p}{w_1} + \lambda_2 \frac{\partial}{\partial q}\frac{\xi_q}{w_2} = 0, \tag{72}$$

$$\lambda_1 \frac{\partial}{\partial p}\frac{\eta_p}{w_1} + \lambda_2 \frac{\partial}{\partial q}\frac{\eta_q}{w_2} = 0, \tag{73}$$

where λ_1 and λ_2 are functions of p and q which are taken proportionally to the squares of the local spacings of the initial grid in Ω:

$$\lambda_1 \sim \|\mathbf{x}_q\|^2, \quad \lambda_2 \sim \|\mathbf{x}_p\|^2. \tag{74}$$

With this choice the ratio λ_1/λ_2 is proportional to the square of the cell aspect ratio:

$$\lambda_1/\lambda_2 \sim \alpha^2. \tag{75}$$

To illustrate the effect of the modification let the edge $q = 0$ in the parametric domain Ω_p represent a solid wall in Ω and let the cells of the initial grid along the wall be orthogonal and have very small aspect ratios, i.e., $\alpha \ll 1$. As a consequence $\lambda_1 \ll \lambda_2$ and the modified equations can be approximated as

$$\frac{\partial}{\partial q}\frac{\xi_q}{w_2} \approx 0, \quad \frac{\partial}{\partial q}\frac{\eta_q}{w_2} \approx 0. \tag{76}$$

Since Neumann boundary conditions are applied we have $\xi_q(p,0) = 0$ and consequently $\xi_q = 0$ for increasing q as long as approximation (76) is valid, i.e., as long as $\lambda_1 \ll \lambda_2$. hence the adapted grid in the boundary layer is nearly orthogonal. A second implication of approximation (72) is that the equation for η (the second equation of (72)) is similar to Eq. (3), Part 1, which shows that the grid in the boundary layer is adapted in normal direction by one-dimensional equidistribution in normal direction of the product $w_2^{-1}\eta_q$.

3.2 Modified equations in the parametric domain: 3D

Following the skewness analysis of section 3.1 we introduce modification functions λ_i, $i = 1,2,3$, to provide orthogonal grids in boundary layers:

$$L_p[\xi] \equiv \lambda_1 \frac{\partial}{\partial p}\frac{\xi_p}{w_1} + \lambda_2 \frac{\partial}{\partial q}\frac{\xi_q}{w_2} + \lambda_3 \frac{\partial}{\partial r}\frac{\xi_r}{w_3} = 0, \tag{77}$$

$$L_p[\eta] \equiv \lambda_1 \frac{\partial}{\partial p}\frac{\eta_p}{w_1} + \lambda_2 \frac{\partial}{\partial q}\frac{\eta_q}{w_2} + \lambda_3 \frac{\partial}{\partial r}\frac{\eta_r}{w_3} = 0, \tag{78}$$

$$L_p[\zeta] \equiv \lambda_1 \frac{\partial}{\partial p}\frac{\zeta_p}{w_1} + \lambda_2 \frac{\partial}{\partial q}\frac{\zeta_q}{w_2} + \lambda_3 \frac{\partial}{\partial r}\frac{\zeta_r}{w_3} = 0. \tag{79}$$

where λ_1, λ_2 and λ_3 are functions of p,q and r which are taken proportionally to the squares of the local spacings of the initial grid in Ω:

$$\lambda_1 \sim \|\mathbf{x}_q\|^2\|\mathbf{x}_r\|^2, \quad \lambda_2 \sim \|\mathbf{x}_p\|^2\|\mathbf{x}_r\|^2, \quad \lambda_3 \sim \|\mathbf{x}_p\|^2\|\mathbf{x}_q\|^2. \tag{80}$$

To illustrate the effect of the modification functions λ_i let the edge $r = 0$ in the parametric domain Ω_p represent a solid wall in Ω and let the cells of the initial grid along the wall be orthogonal and have very small aspect ratios, i.e.,

$$\|\mathbf{x}_r\| \ll \|\mathbf{x}_q\|, \quad \|\mathbf{x}_r\| \ll \|\mathbf{x}_p\|. \tag{81}$$

This situation is illustrated in Fig. 2a. As a consequence $\lambda_1 \ll \lambda_3$ and $\lambda_2 \ll \lambda_3$ and the modified equations can be approximated as

$$\frac{\partial}{\partial r}\frac{\xi_r}{w_3} \approx 0, \quad , \frac{\partial}{\partial r}\frac{\eta_r}{w_3} \approx 0, \quad , \frac{\partial}{\partial r}\frac{\zeta_r}{w_3} \approx 0. \tag{82}$$

Since Neumann boundary conditions are applied we have $\xi_r(p,q,0) = 0$ and consequently $\xi_r = 0$ for increasing r as long as approximation (82) is valid, i.e., as long as $\lambda_1 \ll \lambda_3$ and $\lambda_2 \ll \lambda_3$. The same applies for η_r. Hence the adapted grid in the boundary layer is nearly orthogonal. A second implication of approximation (82) is that the equation for ζ (the third equation of (82)) is similar to Eq. (3), Part 1, which shows that the grid in the boundary layer is adapted in normal direction by one-dimensional equidistribution in normal direction of the product $w_3^{-1}\zeta_r$.

So far the assymptotic behaviour near solid walls with boundary layers is completely similar to the 2D developments. In 3D, however, we have the additional possibility of intersecting solid walls with boundary layers. Suppose that two boundary layers along the boundaries $p = 0$ and $r = 0$ are present, see Fig. 2b. Then in the neighbourhood of the vertex $p = 0$, $r = 0$ we have

$$\|\mathbf{x}_r\| \ll \|\mathbf{x}_q\|, \quad \|\mathbf{x}_p\| \ll \|\mathbf{x}_q\|. \tag{83}$$

As a consequence $\lambda_2 \ll \lambda_1$ and $\lambda_2 \ll \lambda_3$ and the modified equations can be approximated as

$$\lambda_1 \frac{\partial}{\partial p}\frac{\xi_p}{w_1} + \lambda_3 \frac{\partial}{\partial r}\frac{\xi_r}{w_3} \approx 0, \tag{84}$$

$$\lambda_1 \frac{\partial}{\partial p}\frac{\eta_p}{w_1} + \lambda_3 \frac{\partial}{\partial r}\frac{\eta_r}{w_3} \approx 0, \tag{85}$$

$$\lambda_1 \frac{\partial}{\partial p}\frac{\zeta_p}{w_1} + \lambda_3 \frac{\partial}{\partial r}\frac{\zeta_r}{w_3} \approx 0. \tag{86}$$

Hence only one term per equation can be neglected instead of two terms in the previous case of a single boundary layer. Now the question is: will the adapted grid near the vertex be sufficiently orthogonal? This question can only be answered in a qualitative sense since the local solution of the grid adaptation equations depends on the global solution due to the ellipticity of the equations.

To assess the orthogonality question it is convenient to observe the solutions $\xi(p,q,r)$, $\eta(p,q,r)$ and $\zeta(p,q,r)$. As a reference we note that if upon adaptation planes of $p = constant$ are mapped to planes of $\xi = constant$, planes of $q = constant$ are mapped to planes of $\eta = constant$, and planes of $r = constant$ are mapped to planes of $\zeta = constant$, then all angles of the initial grid in the physical domain are conserved within the adapted grid. For the the plane $q = constant$ depicted in Fig. 2b we note that in the neighbourhood of the vertex cells have aspect ratios that are in the order of unity and hence do not differ too much from the corresponding cells in the parametric domain. Hence, if it is assumed that the iso-ξ and iso-ζ surfaces are close to planes of $p = constant$ and $r = constant$ respectively, angles of the initial grid in the physical domain are locally conserved within the adapted grid. Then the question

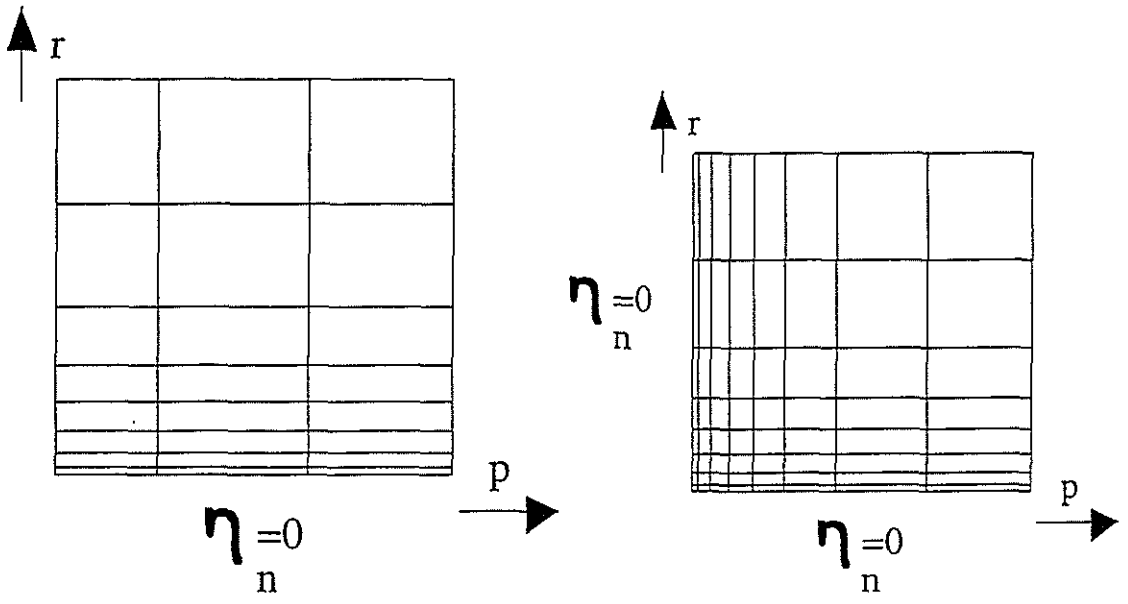

a) Single boundary layer. b) Two intersecting boundary layers.

Figure 2: Schematic impression of single boundary layer and two intersecting boundary layers in an iso-q plane.

remains whether the image of the plane $q = constant$ near the vertex under the adaptive map will be sufficiently close to a plane $\eta = constant$. To answer this question we assume that some distance away from the vertex in the parametric domain, see Fig. 2b, there exists lines in the iso-q plane of $p = \hat{p} > 0$ and $r = \hat{r} > 0$ respectively along which approximations similar to (82) are valid such that η is approximately constant along these lines. Since along curves $p = 0$ and $r = 0$ we have Neumann conditions for η, application of the maximum principle to the enclosed area between these four curves learns that η indeed is approximately constant on the area.

3.3 Discretisation and solution

The differential operator L_p defined by (77) can be approximated by a second-order accurate difference operator L_p^h by replacing derivatives by central differences. In an interior grid point (i, j, k) L_p^h is defined as:

$$L_p^h[.] \equiv \beta_{centre}(.)_{i,j,k} + \beta_{east}(.)_{i+1,j,k} + \beta_{west}(.)_{i-1,j,k}$$
$$+ \beta_{back}(.)_{i,j+1,k} + \beta_{front}(.)_{i,j-1,k} + \beta_{north}(.)_{i,j,k+1} + \beta_{south}(.)_{i,j,k-1}, \tag{87}$$

with

$$\beta_{east} = \frac{1}{\Delta p^2}\frac{2\lambda_1^{i,j,k}}{w_1^{i+1,j,k} + w_1^{i,j,k}}, \quad \beta_{west} = \frac{1}{\Delta p^2}\frac{2\lambda_1^{i,j,k}}{w_1^{i-1,j,k} + w_1^{i,j,k}}, \quad \beta_{back} = \frac{1}{\Delta q^2}\frac{2\lambda_2^{i,j,k}}{w_2^{i,j+1,k} + w_2^{i,j,k}},$$
$$\beta_{front} = \frac{1}{\Delta q^2}\frac{2\lambda_2^{i,j,k}}{w_2^{i,j-1,k} + w_2^{i,j,k}}, \quad \beta_{north} = \frac{1}{\Delta r^2}\frac{2\lambda_3^{i,j,k}}{w_3^{i,j,k+1} + w_3^{i,j,k}}, \quad \beta_{south} = \frac{1}{\Delta r^2}\frac{2\lambda_3^{i,j,k}}{w_3^{i,j,k-1} + w_3^{i,j,k}},$$

$$\beta_{centre} = -(\beta_{east} + \beta_{west} + \beta_{north} + \beta_{south} + \beta_{front} + \beta_{back}) \tag{88}$$

where the subscripts and superscripts i, j, k indicate at which node the functions are evaluated, with Δp, Δq and Δr the mesh sizes of the uniform grid in the parametric domain. The normal derivatives at the boundary $\partial\Omega_p$ are approximated by first order accurate one-sided differences.

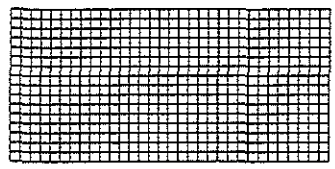

a) Initial grid.

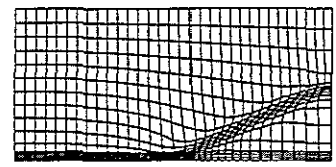

b) Grid after one adaptation.

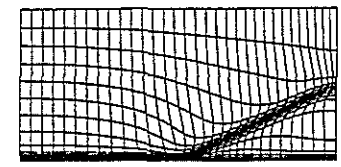

c) Grid after two adaptations.

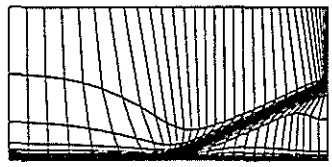

d) Grid after ten adaptations.

Figure 3: Initial grid and adapted grids for oblique-shock boundarylayer simulation.

The above described large linear system is solved by means of GMRES relaxation [17]. The specific GMRES algorithm has been taken from the netlib.linalg library (ftp address: netlib2.cs.utk.edu) provided by the University of Tennessee and Oak Ridge National Laboratory. A correction storage multi-grid technique [18] with fixed V-cycles is used to increase the rate of convergence.

Solution of the MAD equations results in the inverse adaptation map $\xi(\mathrm{p})$. To re-invert this map to the adaptation map $\mathrm{p}(\xi)$ each of the rectangular cells in the uniform 3D grid in the parametric domain Ω_p is subdivided into six tetrahedra. Then in a loop over these tetrahedra the values of ξ, η and ζ are examined at the vertices resulting in a number of candidate new grid points that may be present in the specific tetrahedron. The final presence check only involves some basic linear algebra if all functions on the tetrahedron are linearly approximated.

3.4 Application to a model problem

As a first example, the adaptation algorithm described in the previous section is applied to a model problem that simulates the interaction of an oblique shock and a boundary layer represented by a single scalar function $u(x, y)$,

$$u(x, y) = \tanh(10y) - \tanh(5(x - 2) - 10y), \tag{89}$$

on the rectangular domain $0 \leq x \leq 4$, $0 \leq y \leq 2$. The weight functions employed are:

$$w_1 = \sqrt{1 + {u_x}^2}, \quad w_2 = \sqrt{1 + {u_y}^2}. \tag{90}$$

The modification functions employed are:

$$\lambda_1 = \|\mathrm{x}_q\|^2, \quad \lambda_2 = \|\mathrm{x}_p\|^2. \tag{91}$$

The initial grid of 32x16 cells and a surface plot of the function u are shown in Fig. 3.a. Figures 3.b-3.d show the grid after 1,2, and 10 adaptations, respectively, where the first adapted grid is taken as the initial grid for the second adaptation, the second adapted grid is taken as the initial grid for the third adaptation and so on. The first adapted grid shows the cell concentration at both the "shock" and the "boundary layer". The effects of piecewise bilinear interpolation can be observed in the boundary layer and some wiggles seem to be present which may be caused by even-odd decoupling of the discrete

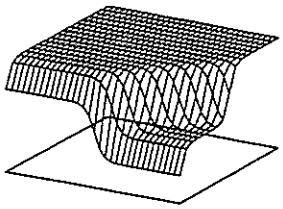

a) Initial solution.

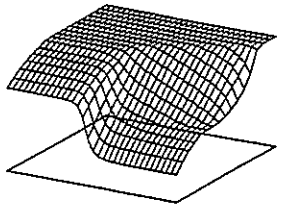

b) After one adaptation.

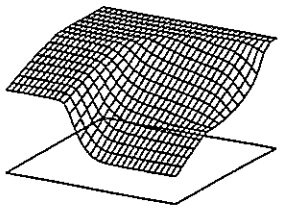

c) After two adaptations.

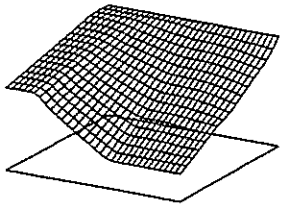

d) After ten adaptations.

Figure 4: Scalar monitor function $u(x, y)$ in the computational domains associated with the initial and adapted grids for oblique-shock boundarylayer simulation.

differential equations. These are minor drawbacks, however, and the adapted grid is acceptable. More adaptation cycles result in stronger cell concentrations and skew cells at the "shock", but they also show the robustness of the algorithm since the last adapted grid (Fig. 3.d) is still a regular non-overlapping grid. Figures 4.a-4.d show the function u in the computational domains associated with the initial grid and the grids after 1,2, and 10 adaptations, respectively. Already after one adaptation the gradient of u in the computational domain decreases significantly, and after 10 adaptations the "shock" and the "boundary layer" almost disappear. Finally it may be noted that the first adaptation is the most effective one, see Figs. 4.a-4.d, while the following adaptations show less dramatic effects.

3.5 Application to a 2D aerodynamic problem: RAE2822 airfoil

The present section presents the adaptation of a C-topology grid around the RAE2822 airfoil suitable for solution of the Reynolds-Averaged Navier-Stokes equations. The flow conditions are transonic: $M_\infty = 0.725$, $Re_\infty = 6.5 \times 10^6$, $\alpha = 2.44^\circ$. The structured C-topology grid consists of 352×64 cells with 256 along the airfoil, 48 cells at both sides of the wake line, and 64 cells in the normal direction to both the airfoil and the wake line. The flow equations are solved with a vertex-based central-difference scheme combined with a modified Baldwin-Lomax turbulence model, described by Brandsma [19]. The weight functions employed are:

$$w_1 = \sqrt{1 + \|Q_p\|^2}, \quad w_2 = \sqrt{1 + \|Q_q\|^2}, \tag{92}$$

where Q is the state vector of flow variables:

$$Q = (\rho, \rho u, \rho v, \rho E)^T, \tag{93}$$

Preliminary to a discussion of the adaptation results we start by choosing the appropriate form of the modification functions λ_i, $i = 1, 2$, that control the adaptation equations in the boundary layer (see (72). Fig. 5a shows the initial grid around the nose of the RAE2822 airfoil showing the initially highly stretched grid at the location where the boundary layer is expected to develop. Fig. 5b shows the adapted grid using $\lambda_1 \equiv 1$, $\lambda_2 \equiv 1.$. It can be observed that the grid indeed is strongly adapted to the expansion region on top of the nose, but is associated with highly skewed cells. This is in agreement with the analysis of section 3.1.

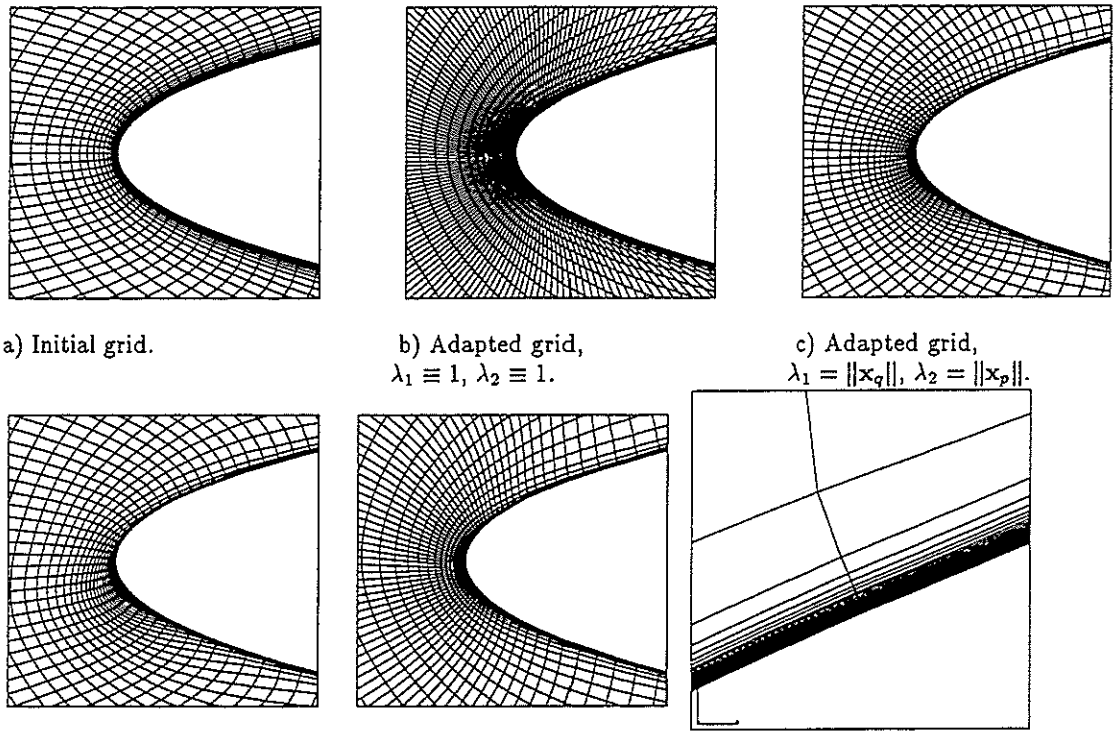

a) Initial grid.

b) Adapted grid, $\lambda_1 \equiv 1$, $\lambda_2 \equiv 1$.

c) Adapted grid, $\lambda_1 = \|x_q\|$, $\lambda_2 = \|x_p\|$.

d) Adapted grid, $\lambda_1 = \|x_q\|^2$, $\lambda_2 = \|x_p\|^2$.

e) Adapted grid, $\lambda_1 = w_1^2\|x_q\|$, $\lambda_2 = w_2^2\|x_p\|$.

f) Adapted grid, close-up showing orthogonality.

Figure 5: Initial and adapted grids around nose of RAE2822 airfoil using different modeling of the modification functions.

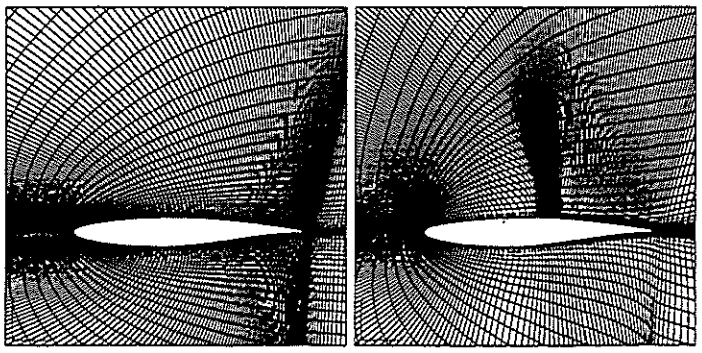

a) Initial grid (352 × 64 cells).

b) Adapted grid (352 × 64 cells).

Figure 6: Initial and adapted grid around RAE2822 airfoil (transonic flow conditions: $M = 0.725$, $Re = 6.5 \times 10^6$, $\alpha = 2.44^{\circ}$).

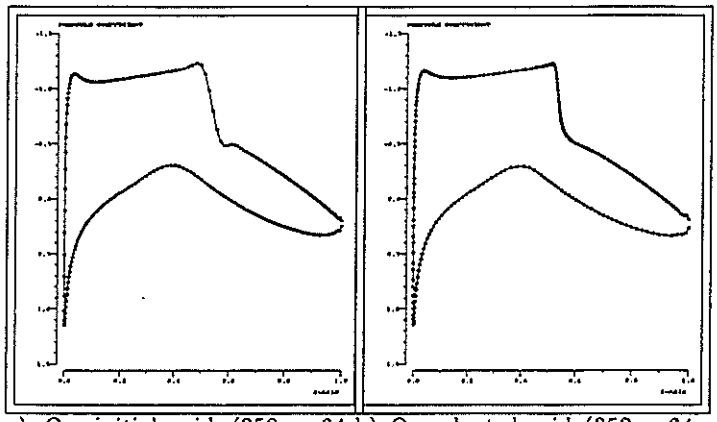

a) On initial grid (352 × 64 cells). b) On adapted grid (352 × 64 cells).

Figure 7: Pressure distributions calculated on initial and adapted grid around RAE2822 airfoil (transonic flow conditions: $M = 0.725$, $Re = 6.5 \times 10^6$, $\alpha = 2.44^{\circ}$).

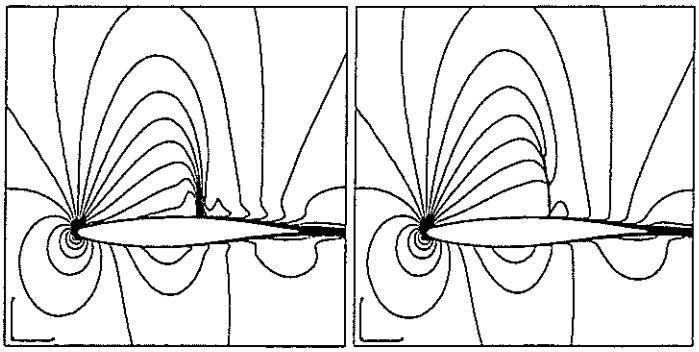

a) On initial grid (352 × 64 cells). b) On adapted grid (352 × 64 cells).

Figure 8: Mach number distributions calculated on initial and adapted grid around RAE2822 airfoil (transonic flow conditions: $M = 0.725$, $Re = 6.5 \times 10^6$, $\alpha = 2.44^{\circ}$).

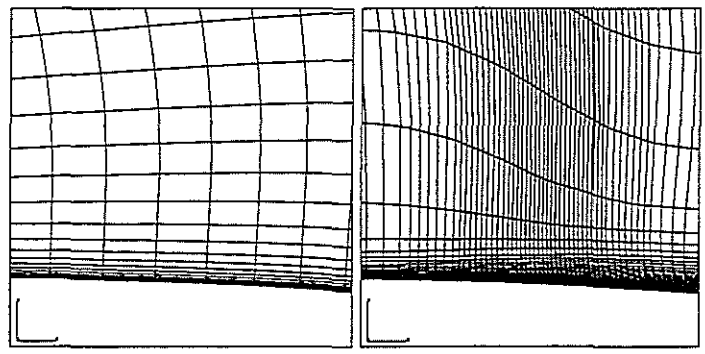

a) Initial grid (352 × 64 cells). b) Adapted grid (352 × 64 cells).

Figure 9: Shock-region close-up of initial and adapted grid around RAE2822 airfoil (transonic flow conditions: $M = 0.725$, $Re = 6.5 \times 10^6$, $\alpha = 2.44^{\cdot}$).

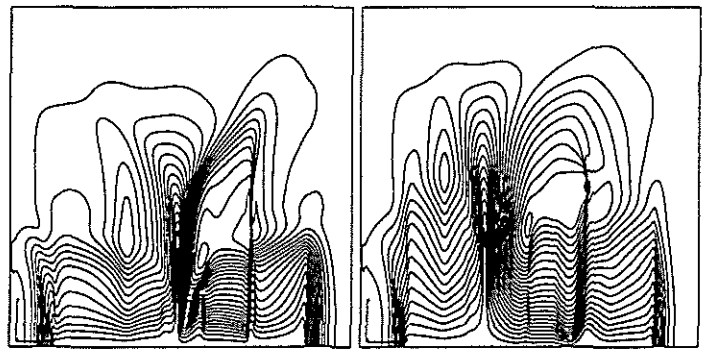

a) On initial grid (352 × 64 cells). b) On adapted grid (352 × 64 cells).

Figure 10: Mach number distributions in the computational domain calculated on initial and adapted grid around RAE2822 airfoil (transonic flow conditions: $M = 0.725$, $Re = 6.5 \times 10^6$, $\alpha = 2.44^{\cdot}$).

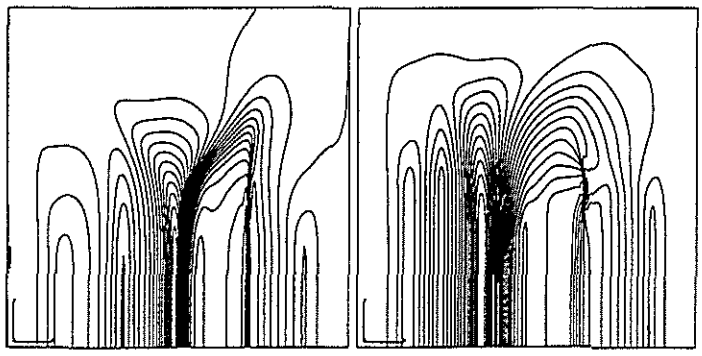

a) On initial grid (352 × 64 cells). b) On adapted grid (352 × 64 cells).

Figure 11: Pressure distributions in the computational domain calculated on initial and adapted grid around RAE2822 airfoil (transonic flow conditions: $M = 0.725$, $Re = 6.5 \times 10^6$, $\alpha = 2.44^{\cdot}$).

When $\lambda_1 = \|x_q\|$, $\lambda_2 = \|x_p\|$ is chosen, see Fig. 5c, the adapted grid outside the boundary layer region is improved significantly with respect to skewness; however, inside the boundary layer (not shown) the grid is still skew. When $\lambda_1 = \|x_q\|^2$, $\lambda_2 = \|x_p\|^2$ is chosen, see Fig. 5d the adapted grid is also orthogonal inside the boundary layer region (not shown) while the grid adaptation in normal direction to the airfoil dominates. But this unfortunately results in excessive depletion of cells in the tangential direction; compare Figs. 5a, 5b and 5d. In order to obtain both one-dimensional equidistribution in the normal direction inside the boundary layer region as well as adaptation in the tangential direction controlled by the outer flow at the edge of the boundary layer, the following choice for the modifications is proposed:

$$\lambda_1 = w_1^2\|x_q\|^2, \quad \lambda_2 = w_2^2\|x_p\|^2. \tag{94}$$

Because just outside the boundary layer the component of the flow solution gradient in normal direction is much smaller than the flow solution gradient in tangential direction ($w_2 \ll w_1$), the tangential adaptation dominates over the normal adaptation when $\|x_q\|/\|x_p\|$ is not too small. The resulting adapted grid is depicted in Fig. 5e, which shows that grid lines normal to the airfoil enter the boundary layer region orthogonally while around the leading edge the grid is also significantly refined in the tangential direction, compare Figs. 5a and 5e. Inside the boundary layer region the adapted grid is also orthogonal, see Fig. 5f. Hence choice (94) for the modification functions is used in the remainder of this section. Large parts of the initial and adapted grid are shown in Fig. 6. The execution time needed to solve the adaptation equations and to invert the inverse adaptation map amounts about 75 CP seconds on the *NEC SX-3 supercomputer (single processor), used for 1254 V-cycles on the ξ-equation, 974 V-cycles on* the η-equation, and 961 iterations on the inversion equations to decrease the maximum residuals 11, 12, and 14 orders of magnitude, respectively. The pressure distributions along the airfoil surface are shown in Figs. 7a-b , and the Mach number contours are given in Figs. 8a-b. A close-up of the grid in the shock region near the airfoil is presented in Fig. 9. Both the shock and the leading edge expansion are better resolved on the adapted grid. Behind the shock the probably spurious kink in the pressure distribution has disapeared. The Mach number distribution just outside the boundary layer has become more uniform in the normal direction. The lift coefficient changed from 0.7714 to 0.7926 (2.7%), the drag coefficient changed from 0.01259 to 0.01248 (1 count), and the pitching coefficient changed from -0.09125 to -0.09399 (3%).

Finally it is interesting to see how the the flow solution in the computational domain changes due to adaptation of the grid and recalculation of the flow. In Figs. 10a-10b the Mach number distribution is depicted in the computational domain. Both the expansion region at the leading edge and the boundary layer are more smoothly distributed in the adapted case (Fig. 10b). The shock has smeared out and the shock in the inviscid outer flow has been regenerated by recalculation of the flow. An exception is the trailing edge region where the gradients in the computational domain are increased upon grid adaptation in the lowest part of the boundary layer. This is probably caused by the modification function λ_1, which is less sensitive for the flow gradient component in tangential direction when the grid has locally very high cell aspect ratios while outside the boundary layer the flow gradient is relatively small. In Figs. 11a-11b the pressure-coefficient distributions in the computational domain is depicted. The same effects as for the Mach number distributions can be observed.

3.6 Application to a 3D aerodynamic problem: ONERA M6 wing

To illustrate the grid adaptation algorithm we present calculations for the ONERA M6 wing under transonic flow conditions [20]. We have performed calculations on both non-adapted and adapted grids, medium and fine grids, and for three different Reynolds numbers, see table 2. For all calculations we

Table 2: Calculated cases for ONERA M6 wing (n=non-adapted, a=adapted).

	dimensions	$Re_\infty = 3 \cdot 10^6$	$Re_\infty = 11.7 \cdot 10^6$	$Re_\infty = 48 \cdot 10^6$
medium	128x24x32	n+a	n+a	n+a
fine	256x48x64	n	n	n

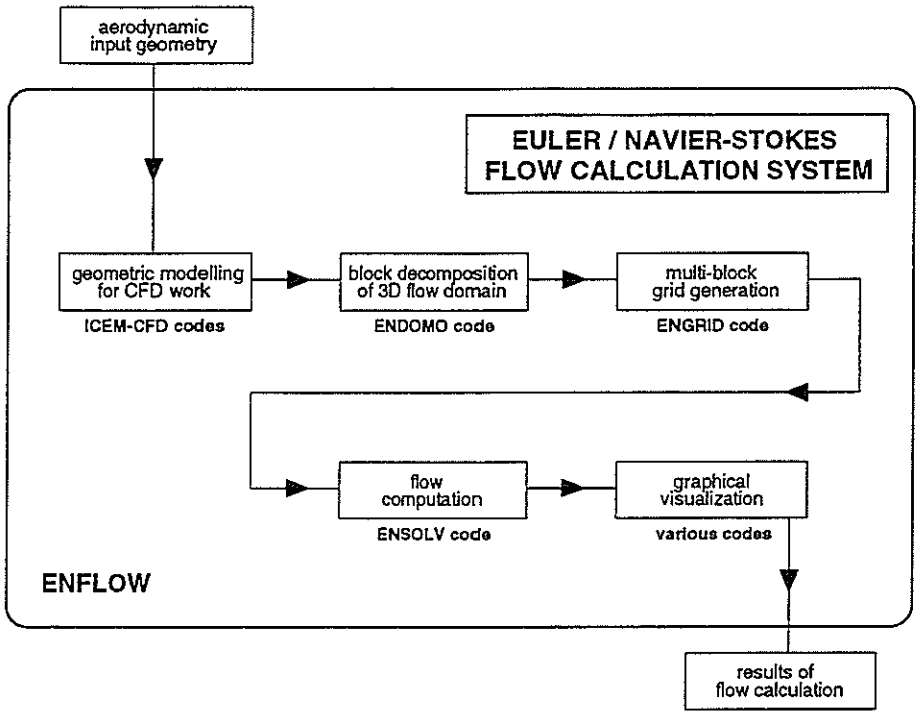

Figure 12: The NLR ENFLOW system

have used the NLR flow simulation system ENFLOW, [21],[22],[23], to calculate the flow solutions on the various grids, or to generate an initial grid. A schematic overview of the NLR ENFLOW system is presented in Fig. 12. The weight functions employed are:

$$w_1 = \sqrt{1 + \|Q_p\|^2}, \quad w_2 = \sqrt{1 + \|Q_q\|^2}, \quad w_3 = \sqrt{1 + \|Q_r\|^2}, \tag{95}$$

where Q is the state vector of flow variables:

$$Q = (\rho, \rho u, \rho v, \rho w, \tilde{p})^T, \tag{96}$$

Fig. 13 shows the medium grid (Fig. 13a) and the adapted medium grid (Fig. 13b) and the calculated pressure coefficient (C_p) distributions (Fig. 13c and 13d). Adaption at the leading edge, trailing edge, shock position and tip are visible resulting in a more pronounced shock. Details of the adaptation near the nose at the symmetry plane (Fig. 13e and 13f) show concentration at the boundary layer with a non-smooth transition to the outer flow.

The C_p distributions at the upper side of various cross sections of the wing are depicted in more detail in Fig. 14 and compared to the fine grid result and experimental data. The suction peak at the leading edge and the down stream expansion zone from the fine grid result and the experimental data is completely recovered by the adapted medium grid result, while the non-adapted medium grid result fails in this respect. The lower side distributions (not shown) show the same features.

The skin-friction (C_f) distributions at the upper side of various cross sections of the wing are depicted in Fig. 15 for the $Re_\infty = 48 \cdot 10^6$ calculation. Along the complete upper side adaptation results in significant improvements. Also it is visible how the laminar-turbulent transition line has shifted upstream upon adaptation due the fact that the flow solver uses grid line indices for transition indication.

The influence of grid adaptation on the boundary layer resolution is explicitly demonstrated in Fig. 16 showing the 'Law-of-the-wall' coordinate Y^+ of the first grid point above the wing surface at the 65% span cross section. For the $Re_\infty = 11.7 \cdot 10^6$ case the Y^+ distribution over the grid is significantly improved upon adaptation compared to the fine grid result. For the $Re_\infty = 48 \cdot 10^6$ case the improvement

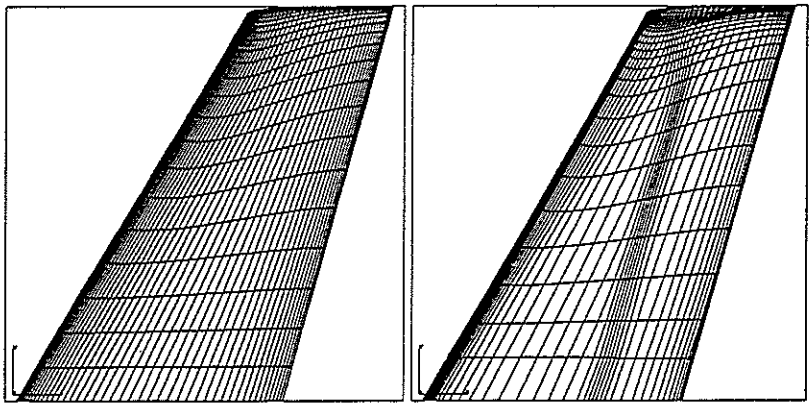

a) non-adapted grid b) adapted grid

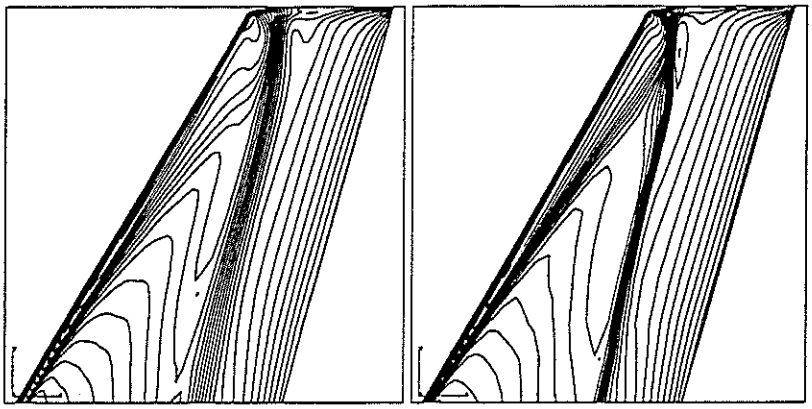

c) C_p on non-adapted grid d) C_p on adapted grid

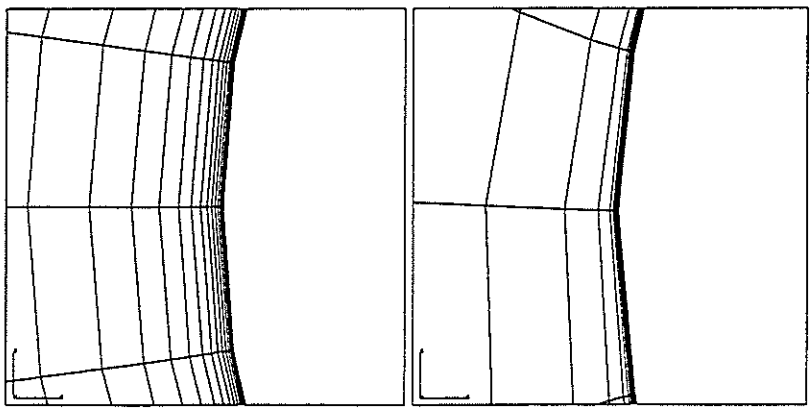

e) non-adapted grid, nose f) adapted grid, nose

Figure 13: Non-dapted and adapted medium grid (a),(b), and C_p-distributions (c) and (d) on wing upper surface, and close-ups of non-adapted and adapted grid near the leading edge in the symmetry plane, $Re_\infty = 11.7 \cdot 10^6$.

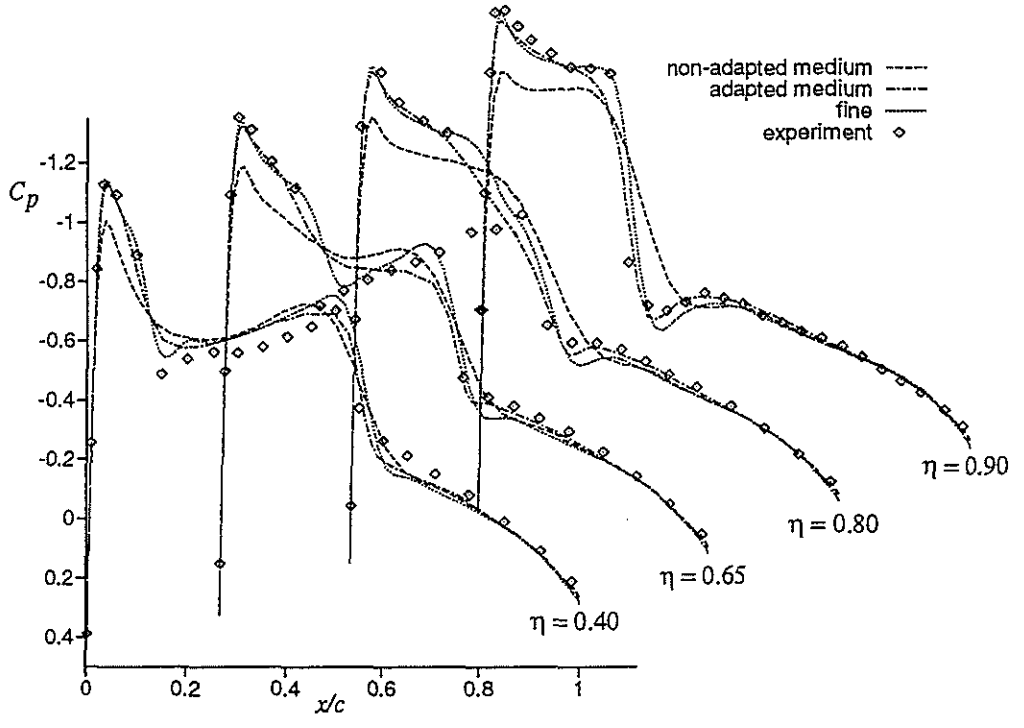

Figure 14: Pressure distributions (C_p) on non-adapted and adapted grids compared to fine grid result and experimental data, $Re_\infty = 11.7 \cdot 10^6$.

is even stronger: the adapted medium grid resolves the boundary layer better than the fine grid and the Y^+ values are roughly reduced by 30%. The stronger effect for the high Reynolds number case is not unexpected since the initial grids have been generated for the $Re_\infty = 11.7 \cdot 10^6$ case by CFD experts with a state-of-the-art elliptic grid generator. From Fig. 16a we learn that even such a special purpose grid can be automatically modified to improve the Y^+ resolution by roughly 50%.

The influence of grid adaptation on the aerodynamic coefficients is shown in Fig. 17 which shows the lift (C_L), drag (C_D), friction drag (C_Df), and pitching moment (C_M) coefficients respectively as calculated on the non-adapted and adapted medium grids, and on the fine grid, for three different Reynolds numbers. Globally grid adaptation results in improvement of the coefficient predictions if compared to the fine grid results. More specifically the drag coefficient, see Fig. 17b, is strongly improved: the gap of 25 counts between the medium and fine grid results is reduced to 6 counts upon grid adaptation. This is still too large for practical problems but it should be reminded that the medium grid only consists of about 100,000 points. Especially the friction drag is improved upon grid adaptation, see Fig. 17c, and only differs by one count from the fine grid result. Besides the absolute values of the predictions it is remarkable that the adapted medium grid results and the fine grid results have the same dependency on the Reynolds number and only differ by a constant for all four coefficients. This is not true for the non-adapted medium grid result.

3.7 Conclusions

A number of grid adaptation methods from the literature have been discussed in the frame work of Weighted Least Squares formulations. The presented compound WLS formulation satisfies all of four formulated requirements including that the natural boundary condition be satisfied. Also a complete interpretation of the functional associated with 3D problems is given which shows that one-dimensional equidistribution is the underlying principle. Application to high Reynolds-number flow calculation requires that the PDE's be modified to explicitely account for orthogonality in boundarylayers, meaning

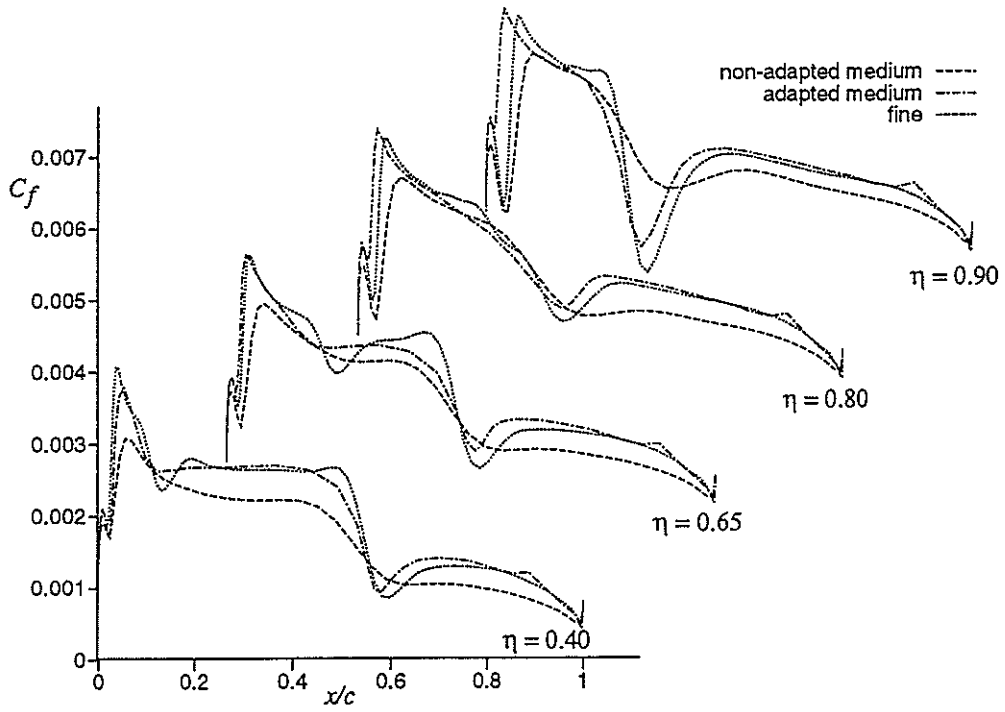

Figure 15: Skin-friction distribution on non-adapted and adapted grids compared to fine grid result, $Re_\infty = 48 \cdot 10^6$

that the functional is not strictly minimised anymore.

Application to 2D and 3D aerodynamic problems consisting of an airfoil and a wing in transonic flow has been demonstrated. Three main conclusions can be drawn:

1. The grid adaptation algorithm enables flow calculations with improved accuracy,
2. The grid adaptation algorithm enables automatic construction of a suitable grid for a wide range of Reynolds numbers,
3. The grid adaptation algorithm enables an improved estimate of the influence of Reynolds number variations on the aerodynamic coefficients.

References

[1] R. Hagmeijer. Grid adaption based on modified anisotropic diffusion equations formulated in the parametric domain. *Journal of Computational Physics*, 115:169–183, 1994.

[2] R. Hagmeijer. Anisotropic grid adaption based on diffusion equations. In *4th International Conference on Numerical Grid Generation in Computational Fluid Dynamics and Related Fields*, Swansea, April 1994.

[3] R. Hagmeijer and J.C. Kok. Adaptive 3d single-block structured grids for the computation of viscous flows around wings. In *5th International Conference on Numerical Grid Generation in Computational Fluid Dynamics and Related Fields*, Starkville, Mississippi, April 1-5 1996.

[4] R. Hagmeijer. *Adaptation of Structured Grids Based on Weighted Least Squares Formulations (in progress)*. PhD thesis, Technical University of Delft, Delft, The Netherlands.

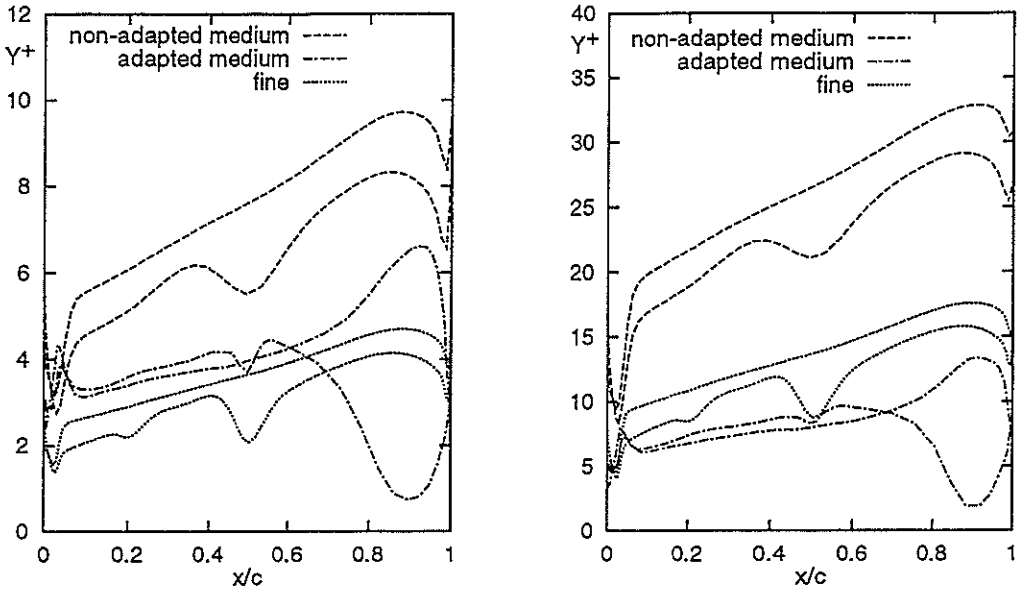

a) $Re = 11.7 \cdot 10^6$ b) $Re = 48 \cdot 10^6$

Figure 16: Law-of-the-wall coordinate of first grid point above the surface at 65% span cross section on various grids.

[5] D.M. Young. *Iterative Solution of Large Linear Systems.* Academic Press, New York and London, 1971.

[6] R. Courant and D. Hilbert. *Methods of Mathematical Physics*, volume I. Wiley, New York, 1989.

[7] M.H. Protter and H.F. Weinberger. *Maximum Principles in Differential Equations.* Prentice Hall, Englewood Cliffs N.J., 1967.

[8] J.U. Brackbill and J.S. Saltzman. Adaptive zoning for singular problems in two dimensions. *Journal of Computational Physics*, 46:342–368, 1982.

[9] A. Winslow. *Adaptive Mesh Zoning by the Equipotential Method.* UCID-19062, Lawrence Livermore National Laboratories, 1981.

[10] P.R. Eiseman. Adaptive grid generation. *Computer Methods in Applied Mechanics and Engineering*, 64:321–376, 1987.

[11] A.S. Dvinsky. Adaptive grid generation from harmonic maps on Riemannian manifolds. *Journal of Computational Physics*, 95:450–476, 1991.

[12] J.U. Brackbill. An adaptive grid with directional control. *Journal of Computational Physics*, 108:38–50, 1993.

[13] S.P. Spekreijse, R. Hagmeijer, and J.W. Boerstoel. Adaptive grid generation by using the Laplace-Beltrami operator on a monitor surface. In *5th International Conference on Numerical Grid Generation in Computational Fluid Dynamics and Related Fields*, Starkville, Mississippi, April 1-5 1996.

[14] Ph. Clement, R. Hagmeijer, and G. Sweers. On the invertibility of mappings arising in 2D grid generation problems. *to be published in Numerische Matematik*, -:–, 1995.

[15] D. Gilbarg and N.S. Trudinger. *Elliptic partial differential equations of second order*, volume 2^{nd} edition. Springer Verlag, Berlin, Heidelberg, New York, Tokyo, 1983.

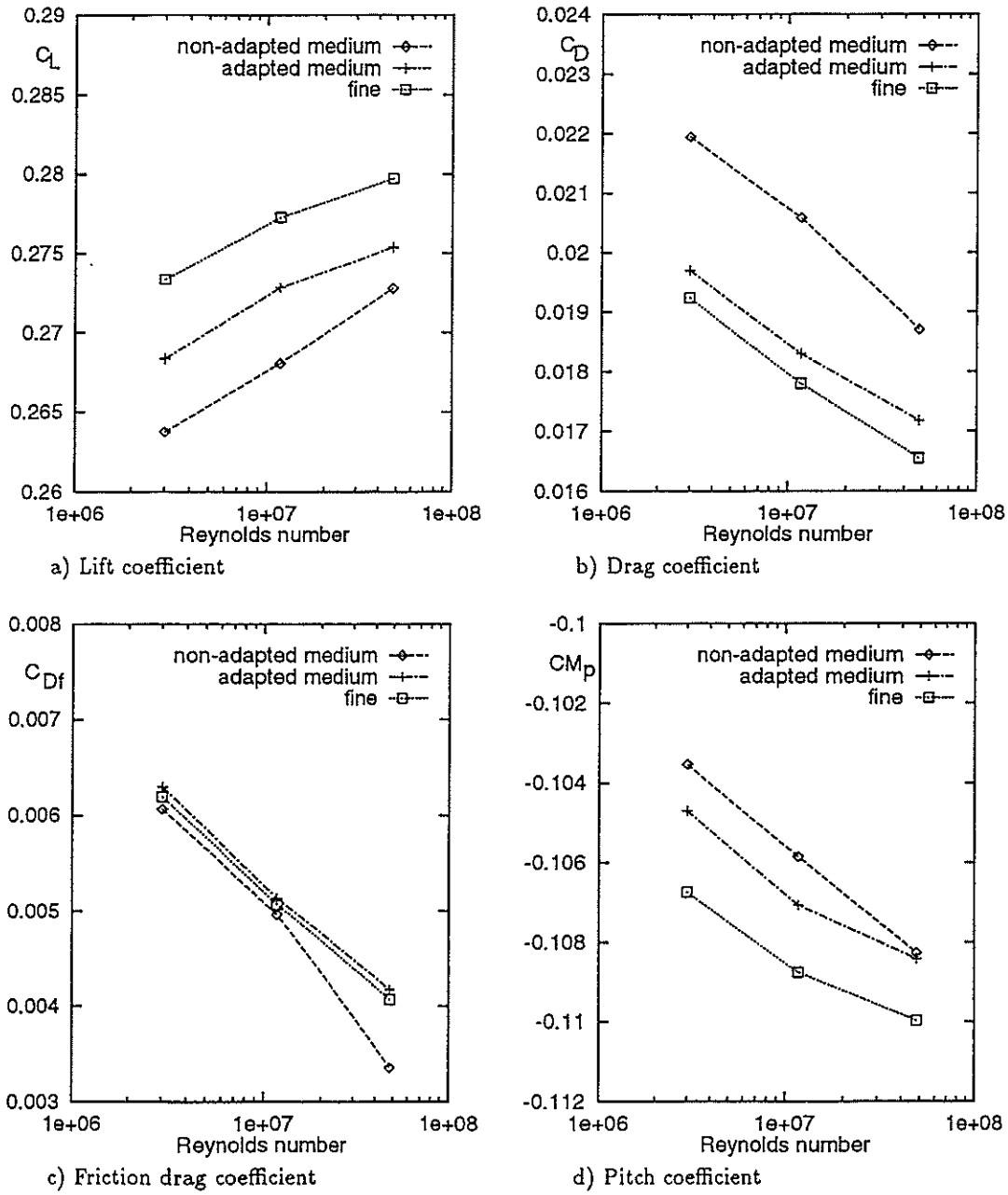

a) Lift coefficient

b) Drag coefficient

c) Friction drag coefficient

d) Pitch coefficient

Figure 17: Force coefficients as function of Reynolds number calculated on non-adapted and adapted medium grids, and calculated on fine grid.

[16] F. Schulz. *Regularity theory for quasilinear elliptic systems and Monge-Ampēre Equations in two dimensions*, volume 1445. Springer Lecture Notes, 1990.

[17] R. Barrett, M. Berry, T. Chan, J. Demmel, J. Donato, J. Dongarra, V. Eijkhout, R. Pozo, C. Romine, and H. van der Vorst. *Templates for the Solution of Linear Systems: Building Blocks for Iterative Methods*. SIAM Publications, 1993.

[18] A. Brandt. Multi-level adaptive solutions to boundary-value problems. *Mathematics of computation*, 31(138):333–390, 1977.

[19] F.J. Brandsma. in: Euroval-a European initiative on validation of CFD codes, ed. W. Haase et. al. *Notes on numerical fluid mechanics*, 42, 1993.

[20] V. Schmitt and F. Charpin. *Experimental Data Base for Computer Program Assessment*, volume AGARD-AR-138. Advisory Group for Aerospace Research & Development, Neuilly-sur-Seine, France, 1979.

[21] J.W. Boerstoel. ENFLOW a system of CFD codes for industrial CFD analysis of flows around aircraft including propulsion systems modelling. Technical Report NLR CR 93519 L, National Aerospace Laboratory, 1993.

[22] S.P. Spekreijse. Elliptic grid generation based on laplace equations and algebraic transformations. *Journal of Computational Physics*, 118:38–61, 1995.

[23] J.C.Kok, M. Amato, S. Bosse, and A. Kassies. Numerical design of ENSOLV; a code for the numerical simulation of 3d flows using the thin-layer Navier-Stokes and Euler equations. Technical Report NLR CR 93152 L, National Aerospace Laboratory, 1993.